Gao et al. Journal of Wood Science (2024) 70:12
https://doi.org/10.1186/s10086-024-02125-5

Journal of Wood Science

ORIGINAL ARTICLE

Open Access

Research on wind pressure characteristics of traditional timber buildings: a case study of the main hall of Shisi Temple

Xiaoyue Gao[1], Qing Chun[1*] and Yidan Han[1]

Abstract

Traditional timber buildings are sensitive to wind action. Studying the wind pressure characteristics is the premise for the preventive conservation of traditional timber buildings. To investigate the computational fluid dynamics (CFD) numerical simulation method for wind pressure on traditional timber buildings, a typical traditional timber building, the main hall of Shisi Temple, is chosen as a case to carry out the study. A comparative analysis is conducted to examine the effects of curve simplification of the roof slope, as well as the Dougong (bracket sets) and roof tile components, on the numerical simulation results of wind pressure on the building surface. Additionally, simplification schemes of geometric modeling are provided for the efficient and accurate simulation. The results indicate that moderate simplification of the roof curve has a relatively minor impact on the overall calculation of wind pressure, and the difference between the drag coefficients of the simplified model and the accurate model is no more than 3%. However, excessive simplification can lead to distorted simulation results, and a three-segment curve simplification method is recommended for roof cornices. The influence of Dougong on the wind pressure calculation results is negligible (within 5%), whereas roof tiles significantly reduce the drag coefficient, with an impact of over 30% at various wind directions. The impact of roof tiles on wind pressure distribution in traditional timber buildings lies in their alteration of the building aerodynamic shape rather than an increase in roof thickness. The findings can provide a basis for assessing the wind resistance of traditional timber buildings and helpful insights for improving the efficiency of wind pressure analyses of traditional timber structures.

Keywords Traditional timber buildings, Wind pressure, CFD, Numerical simulation methods

Introduction

Wooden architectural heritage is a typical type of the world's architectural heritage and can be regarded as a carrier of historical memory, cultural development, and civilization progress [1–6]. Most of the existing ancient wooden buildings are in East Asia (e.g., China, Japan, and Korea). For example, the Horyuji Temple is discovered as the world's oldest timber building which was built in 607 A.D. in Nara of Japan [7]. The Great Buddha Hall of Todaiji Temple in Nara, Japan, is the world's largest surviving wooden structure, with a width of 57.01 m, a depth of 50.48 m, and a height of 48.74 m. These traditional timber buildings are embodied with historical, cultural, and scientific values, so the protection of them is of great importance.

Traditional timber buildings are constructed of wood and researchers have observed that they are susceptible to wind damage. In August 2006, under the influence of super typhoon Sangmei, Ziguo Temple, a famous Buddhist temple in China with a history of more than 1000 years, was severely damaged. The gate tower was blown down and almost all the tiles on all the buildings of the temple were removed. More than 20 traditional

*Correspondence:
Qing Chun
cqnj1979@163.com
[1] School of Architecture, Southeast University, Nanjing, China

timber buildings of the Tang and Song dynasties (618 A.D.–1279 A.D.) in the temple were blown down and almost all of them were destroyed (Fig. 1a). Similarly, in 2018, Super Typhoon Jebi made landfall in western Japan, causing varying degrees of damage to traditional timber buildings in the surrounding area, such as Higashi Honganji Temple, Daigoji Temple, and Nishi Honganji Temple (Fig. 1b). Consequently, an increasing number of researchers have begun studying the wind resistance of traditional timber buildings.

As early as 1991, scholars recognized the impact of wind on traditional timber buildings. Delun et al. [8] conducted wind force experiments on tall wooden pagodas in China and established a wind pressure coefficient for wooden pagodas. Currently, the most comprehensive research on the wind resistance of traditional timber buildings focuses on tall wooden pagodas, specifically the Yingxian wooden pagoda. From 2002 to 2005, Tieying et al. [9, 10] analyzed the wind pressure and wind-induced vibration characteristics of the Yingxian wooden pagoda using theoretical calculations and wind tunnel tests and suggested a possible correlation between gust effects and the remnant deformation of the pagoda. In 2010, Lin'an et al. [11] conducted on-site measurements of the wind environment and surface wind pressures on the Yingxian wooden pagoda, finding that wind loads can further aggravate existing damage and structural tilting of the wooden pagoda, posing a significant threat to its safety. In recent years (2020–2023), extensive research has been conducted by Li et al. and Yuhang et al. [12–16] on the wind resistance performance of the Yingxian wooden pagoda. Their research mainly combines field measurements, wind tunnel tests, and computational fluid dynamics (CFD) numerical simulations to study the wind pressure coefficient and wind pressure distribution of the pagoda. In addition to the Yingxian Wooden Pagoda, the wind performance of Five-Story pagodas has also been studied [17, 18]. Apart from tall structures, many representative low-rise traditional timber buildings have been studied. For example, Xun et al. [19] and Chengjun et al. [20] have studied the wind resistance performance of specific low-height traditional timber buildings such as Dingding Gate, Taihe Hall, Tian'anmen Gate Tower, and Jiayuguan Wooden Fortresses. In general, studies on the wind resistance of traditional timber buildings include wind pressure distribution [21, 22], displacement response [23–25], and wind-induced damage [26–28].

Many scholars have carried out research on the wind resistance of traditional timber buildings, but there is a lack of consideration of simplifying effects of the models analyzed. From the above research status, it can be seen that in the wind resistance research of traditional timber structures, researchers mostly employ the economical and efficient CFD simulation method to obtain the surface wind pressure on the buildings. In CFD simulations, the pre-processing steps such as geometric model creation and grid generation directly affect the calculation quality and efficiency. However, traditional East Asian timber architectural components have complex shapes. For example, traditional architectural features such as overhanging roofs, deep eaves, Dougong (bracket sets), roof tiles, ridge lines, and roof cornices all affect the wind environment around buildings and

a. Ziguo Temple damaged by wind disaster

b. Nishihonganji damaged by wind disaster

Fig. 1 Cases of wind damage in traditional timber buildings

the distribution of wind pressure on their surfaces. These components are crucial factors to consider in wind pressure calculations. However, detailed geometric models can increase the difficulty of grid generation, leading to a significant increase in the number of grids and compromising grid quality, which in turn reduces the efficiency of CFD computations. Therefore, researchers often simplify the shapes of traditional buildings. However, whether these simplifications lead to significant deviations in the calculation results has not been explored. Striking a balance between the accuracy of geometric modeling and the efficiency of computation is meaningful and necessary for numerical simulations of wind pressure on traditional timber structures. Therefore, this study focuses on a geometric modeling strategy for the numerical simulation of wind pressure on traditional timber buildings. Taking the main hall of Shisi Temple in Zhejiang Province as a typical example of traditional timber architecture, this study specifically investigates the influence of roof shape, tiles, Dougong, and other major components on wind pressure calculation results. This paper proposes appropriate geometric modeling methods for numerical simulations of wind pressure. The research findings can provide guidance for establishing geometric models for numerical simulations of wind pressure on traditional timber structures, ensuring calculation accuracy while significantly improving computational efficiency.

Materials

Traditional East Asian architecture is primarily characterized by a timber structural system, and an individual building can be divided into three parts: the platform, the body, and the roof. To protect the timber structure, roofs often have large eaves. However, large eaves can hinder daylight penetration and increase the risk of rainwater erosion on the foundation. Consequently, curved roofs or lift and fold roofs were later adopted along with raised corners, giving the roofs and corners a more lightweight and lively appearance. The traditional roof forms mainly include the Wudian roof (hip roof), the Xieshan roof (hip-and-gable roof), the Xuanshan roof (gable roof with hanging eave), the Yingshan roof (gable roof without hanging eave), and the Cuanjian roof (pavilion roof). Among the existing official-style traditional building remnants in China, the Wudian and Xieshan roofs are the most common, with both having single- and double-eave forms. These include the single-eave Wudian roof (Fig. 2a), double-eave Wudian roof (Fig. 2b), single-eave Xieshan roof (Fig. 2c), and double-eave Xieshan roof (Fig. 2d). In terms of geometric complexity, the double-eave Xieshan roof is the most intricate and has the most significant impact on airflow and wind pressure distribution. The focus of the present study is on the influence of complex component modeling on the quality and efficiency of calculations. From this perspective, the main hall of Shisi Temple, a representative traditional timber building with a double-eave Xieshan roof, was selected as the research subject to obtain more general and typical research results.

Shisi Temple was built during the Southern Song Dynasty (1140 AD). It is located in Lishui City, Zhejiang Province, on the Baixiang Mountain at an altitude of over 1000 m. In 2001, Shisi Temple was announced as the fifth batch of National Key Cultural Heritage sites. The main hall of Shisi Temple is a timber structure composed of three parts: the platform, the body, and the roof (Fig. 3a). Among these, the roof is the most exquisite and complex, featuring a double-eave Xieshan roof. The roof is supported by Dougong (Fig. 3b), covered with tiles (Fig. 3c), and has a smooth and graceful ridge shape. The main hall of Shisi Temple has a width of three bays and a depth of two bays, with a total length of 12 m, width of 12 m, and height of 10.3 m. The geometric information of the main hall is based on 3D scanning results, and the architectural blueprint of the main hall is shown in Fig. 4.

Methods

This study utilized the computational fluid dynamics (CFD) method, which is a technique that can simulate the flow of real fluids. It has unique advantages such as low cost, fast speed, comprehensive data, and the ability to simulate various conditions, making it an important method in structural wind resistance research. Fluent 2022R1 was used to implement the CFD simulation. Three main factors affecting the distribution of surface wind pressures on traditional buildings were considered: (1) roof curve shape, (2) roof tiles, and (3) Dougong. Geometric models of the roof were established using different curve simplification methods to study the shape of the roof curve. The results were calculated, compared, and analyzed to determine the most reasonable curve simplification method. For the study of roof tiles and Dougong, models considering only tiles, only Dougong, and both tiles and Dougong were established, respectively. The results were calculated, compared, and analyzed to assess the influence of different components on the distribution of surface wind pressures on traditional buildings. Reasonable suggestions for geometric model simplification were provided while ensuring calculation quality. Before conducting the aforementioned calculations, grid independence verification was performed.

a. Shanhua Temple (Built in 1128; Located in China; The most well-preserved traditional building of Liao dynasty)

b. Todaiji Temple (Built in 728; Located in Japan; The world's largest surviving wooden structure)

c. Bulguksa Temple (Built in 530; Located in Korea; Known as the most exquisite Buddhist temple in Korea)

d. Shisi Temple (Built in 1140; Located in China; A representative traditional timber building of Song dynasty)

Fig. 2 Typical existing wooden structures

Method reliability verification

In order to ensure the reliability of the research methodology, the accuracy of the CFD method was checked by comparing the CFD calculations with the TPU Aerodynamic Database [29] results before the formal calculations. A low-rise building with eaves that is similar to the main hall of the Shisi Temple was selected for the calculations. As shown in Fig. 5a, the sizes of test gable-roofed low-rise building model were 24 m length (D), 16 m width (B), 6 m height (H0), with roof pitch of 26.7°. The wind velocity was 23.4 m/s at the height of 10 m and the exponent of mean wind velocity profile was 0.20. After comparison, the steady-state calculation with the standard k–ε turbulence model was adopted. As shown in Fig. 5b, c, it can be seen that the CFD calculation results are in good agreement with the wind tunnel test results given in the TPU database. Therefore, the CFD method is reliable and can be used for wind pressure analysis of buildings.

CFD calculation settings

Based on the architectural blueprint, a full-scale geometric model was established as shown in Fig. 6a. The model had a 12 m length, 12 m breadth (B), and 10.3 m height. To ensure the full development of the flow field, an external domain was set up with dimensions of 312 m

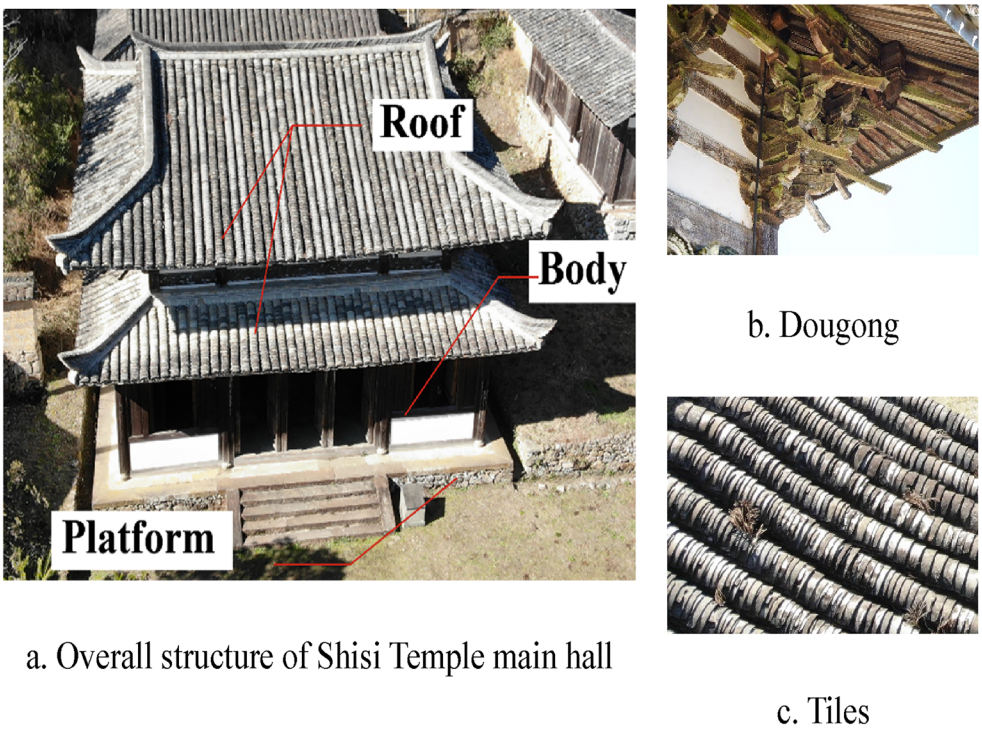

Fig. 3 Architectural structure of the main hall of Shisi Temple

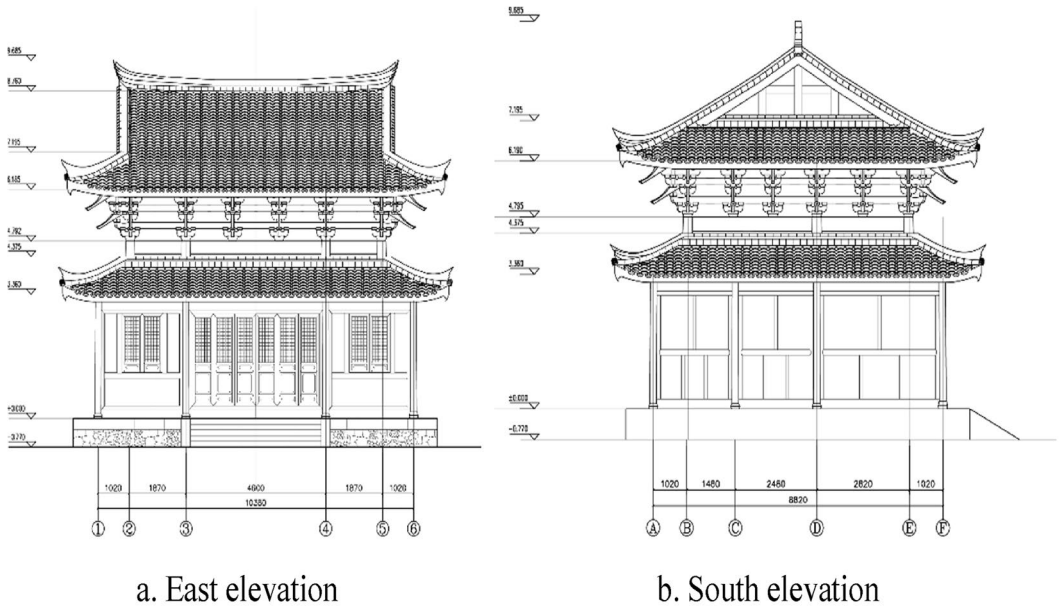

Fig. 4 Architectural blueprint of the main hall of Shisi Temple

in length (26B), 144 m in width (12B), and 72 m in height (6B), as shown in Fig. 6b. The model center was located at a distance of 6B from the entrance of the external domain and 20B from the exit, with a distance of 6B from the sides and top. To calculate the flow field near the model more accurately, an internal domain with dimensions of 72 m in length (6B), 48 m in width (4B), and 24 m in height (2B) was set up around the model. The model

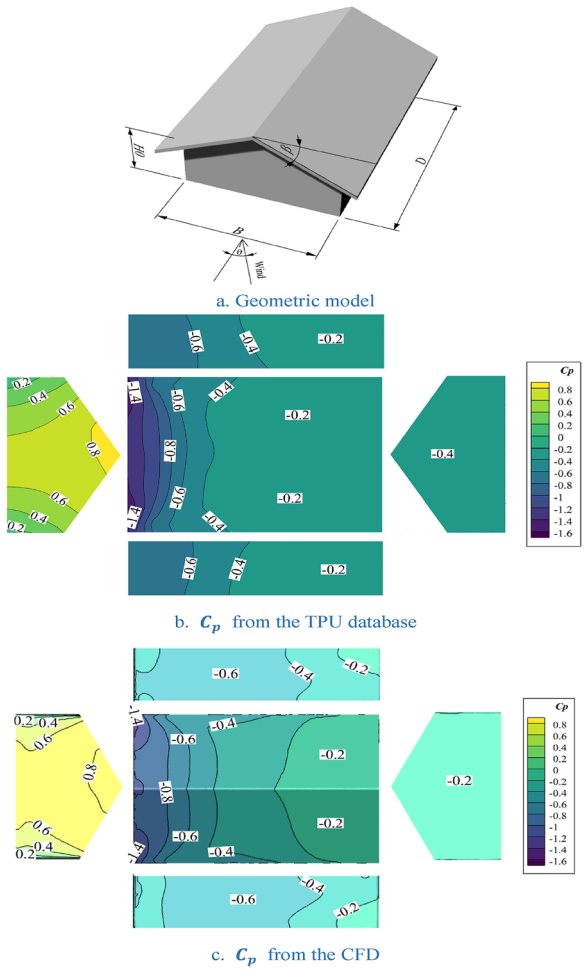

Fig. 5 Comparison of CFD calculation results with TPU database

center was located at a distance of 2B from the entrance of the internal domain and 4B from the exit, with a distance of 2B from the sides and top. The blockage ratio was calculated as 1.19% (< 5%). As shown in Fig. 6b, the entrance of the external domain was set as Velocity Inlet, the exit as Pressure Outlet, the bottom surface as Wall, and the side and top surfaces as Symmetric boundaries. The bottom surface of the internal domain was set as Wall, while the other surfaces were set as interior boundaries. The model surfaces were all set as Wall. This study adopted steady-state calculation with the realizable k–ε turbulence model [16], which performs well in simulating complex structures of traditional timber buildings.

The setting of the incoming flow at the inlet was based on the following:

The wind speed value for a 100-year return period at the Lishui meteorological station in Zhejiang Province was determined to be 29.9 m/s. The vicinity of the temple is characterized by dense vegetation and numerous low-rise buildings. According to the Load Code[30] in China, this type of terrain is classified as Category C, with a corresponding roughness coefficient α of 0.22, and the nominal turbulence intensity at 10 m height is 0.23. The power-law wind velocity profile is presented in Eq. (1), and the distribution of turbulence intensity along the height can be calculated as in Eq. (2). In summary, the inlet wind profile is set up as shown in Fig. 7.

$$U_z = 29.9 \times \left(\frac{Z}{10}\right)^{\alpha} \tag{1}$$

Here, Z is the height (m), and U_Z represents the wind speed (m/s) at height Z.

$$I_z = 0.23 \times \left(\frac{Z}{10}\right)^{-\alpha} \tag{2}$$

Here, I_Z represents the turbulence intensity at height Z.

Grid independence verification

From the principle of the finite-volume method, the finer the grid, the higher the accuracy of the solution is. However, in practical engineering applications, a significant increase in the number of grids results in a substantial increase in the computational time. Moreover, beyond a certain grid quantity threshold, the improvement in computational accuracy becomes less significant. Therefore, a grid meshing that balances the computational accuracy and efficiency is of great significance. Prior to the actual calculations, the influence of grid density on the results must be assessed. Considering the complexity of the model shape and the computational efficiency, both nonstructural and structural grids are used, with nonstructural grids in the internal domain and structural grids in the external domain. As shown in Fig. 8, calculations were performed with various grid meshing schemes consisting of 140,000, 280,000, 580,000, 2,120,000, and 8,020,000 elements, respectively. The drag coefficient C_d was compared among these cases. C_d is a dimensionless quantity in fluid mechanics that represents the resistance of an object in fluid. Its expression is given by Eq. (3).

$$C_\mathrm{d} = \frac{F_\mathrm{d}}{0.5\rho v^2 A}. \tag{3}$$

Here, F_d is the drag force acting on an object; ρ is the incoming flow density, taken as 1.225 kg/m^3; v is the reference velocity at the reference height, the wind speed of 27.75 m/s at a height of 7.12 m (average height of the roofs) is selected for this study; and A is the reference area, which can be referred to as the frontal area or the projected area, taken as 93.3751 m^2.

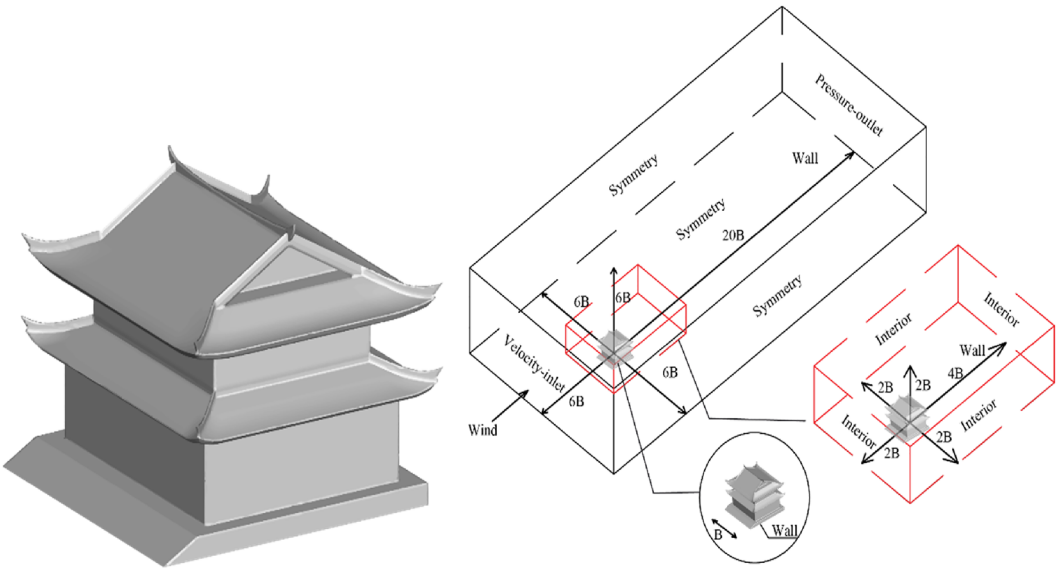

Fig. 6 Geometric model and boundary condition settings

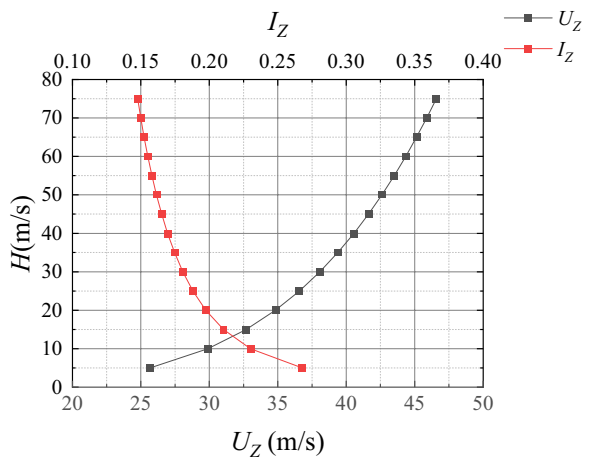

Fig. 7 Profile of mean wind velocity and turbulence intensity at the inlet

The detailed grid sizes are provided in Table 1. It can be observed from the table that the results obtained from the grid of 280,000 to 8,020,000 elements differ by less than 5%, which is within an acceptable range. Considering the balance between computational accuracy and time cost, the final calculation was performed using the grid meshing scheme with 2,120,000 elements.

Models

Roof curve simplification models

The roof cornices in traditional Chinese timber architecture often exhibit varying degrees of curvature, contributing to the grand and elegant appearance of the entire structure. The curved nature of the cornices poses challenges in modeling, as they form spatial curves that are difficult to represent accurately. Many researchers have resorted to simplifying these curves by approximating them with multi-segment straight lines; however, there is currently no universally accepted simplification method. In this regard, this study proposes a method that specifically addresses the simplification of roof cornices in traditional Chinese timber architecture.

In traditional Chinese timber architecture, the cornices often form curves without inflection points. For a curve without inflection points, the following simplifications can be made when modeling the roof:

(a) Determine the modeling accuracy a;
(b) Determine the number n of divisions; divide a curve into n equal segments based on its length;
(c) Draw the multi-segment polyline using $(n+1)$ equally divided points;
(d) Measure in turn the maximum distance d_i from the ith $(i = 1, 2, \ldots, n)$ segment of the line to its corresponding curve, and compare the distance d_i with the determined modeling accuracy a;
(e) If all d_i values are smaller than a, then the simplification of that curve is complete. However, if all

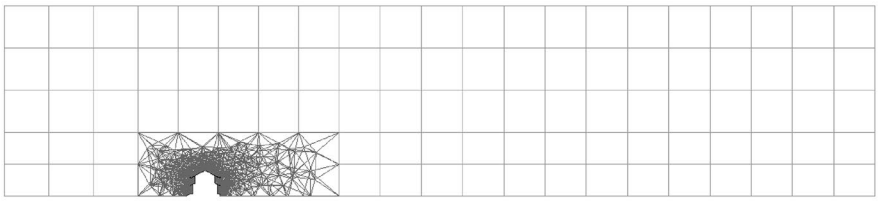

a. 140000 divisions

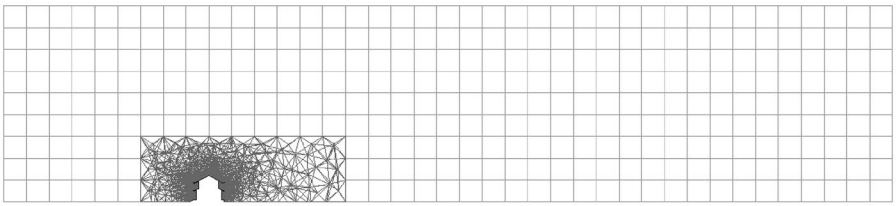

b. 280000 divisions

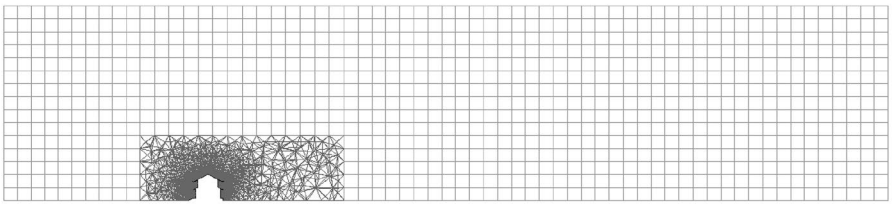

c. 580000 divisions

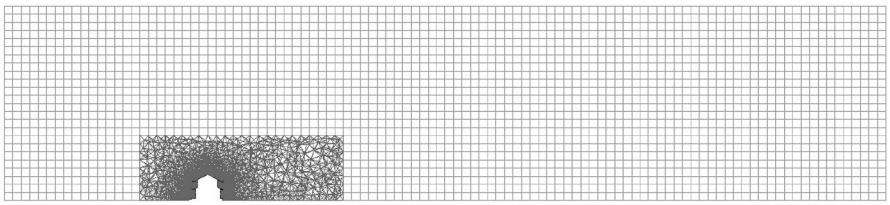

d. 2120000 divisions

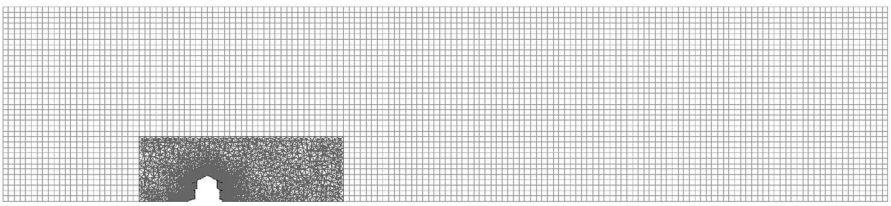

e. 8020000 divisions

Fig. 8 Grid divisions with different meshing schemes

Table 1 Grid size setting

No.	Global Max element (m)	Max element of building (m)	Grid count	C_d	Deviation (%)
1	15	0.5	137,766	0.5164	− 44.04
2	8	0.3	278,549	0.8881	− 3.75
3	5	0.2	577,066	0.8792	− 4.72
4	3	0.1	2,121,623	0.8966	− 2.83
5	2	0.05	8,017,578	0.9228	0.00

d_i values are greater than a, re-evaluate and adjust the number of divisions (n) and return to Step 2. If some d_i values are greater than a, consider those curve segments as the new curves that need to be simplified, then re-evaluate and adjust the number of divisions (n), and return to Step 2. This process continues until all curve segments satisfy the condition $d_i < a$ ($\max d_i < a$);

(f) Replace the original curve with the simplified multi-segment polyline.

A precise model of the main hall of Shisi Temple was created using Rhino7.0. Additionally, based on the principles described above, simplified models can be created with accuracies of 50 mm ($a=50$ mm, $n=3$, using a 3-segment polyline to approximate the roof cornices) and 200 mm ($a=200$ mm, $n=2$, using a 2-segment polyline to approximate the roof cornices). The resulting models are shown in Fig. 9.

Models with different components

Roof tiles and Dougong are often overlooked in modeling because of their complex geometries and relatively small volumes. However, they are located in close proximity to the roof and can potentially affect the wind pressure on the roof. Considering that roof pressure is a crucial factor in assessing the wind resistance of traditional buildings, it is important to investigate the impact of roof tiles and Dougong on wind pressure calculation results. Therefore, geometric models were created to separately consider the effects of roof tiles, Dougong, and their combination. Recognizing the intricate details of roof tiles and Dougong with high-accuracy models would significantly increase the number of computational grids; therefore, the effects of different components were analyzed based on the 200-mm-accuracy model. The three geometric models that consider the different components are shown in Fig. 10. In the model, the upper and lower tiles were modeled as a whole with a total thickness of 0.14 m. And the Dougong was divided into column Dougong and corner Dougong, of which the width of column Dougong was 0.80 m, the width of corner Dougong was 1.50 m, and their height was 1.56 m.

Calculation conditions

Considering that the influence of model accuracy on the calculation results may vary at different wind directions, the wind pressure was calculated for different accuracy models at wind directions of 0°, 45°, 90°, 135°, and 180°. A schematic of the wind directions α is shown in Fig. 11.

Results and discussion

The influence of roof shape simplification on wind pressure calculation results

Figure 12 shows the CFD simulation results for the accurate model at a wind direction of 0°. From the Fig. 12a, it can be observed that the windward surface of the building takes predominantly positive pressure, whereas the side and leeward surfaces take negative pressure. It can be noted that the maximum positive wind pressure is found between the first and second

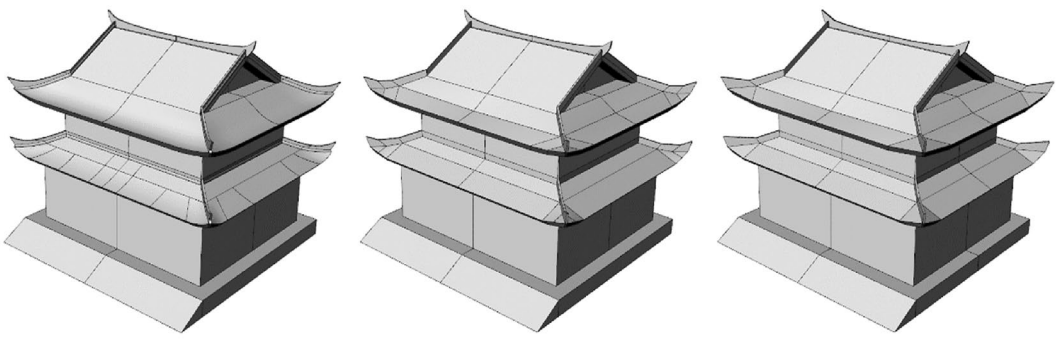

Fig. 9 Illustrations of geometric models with different accuracies

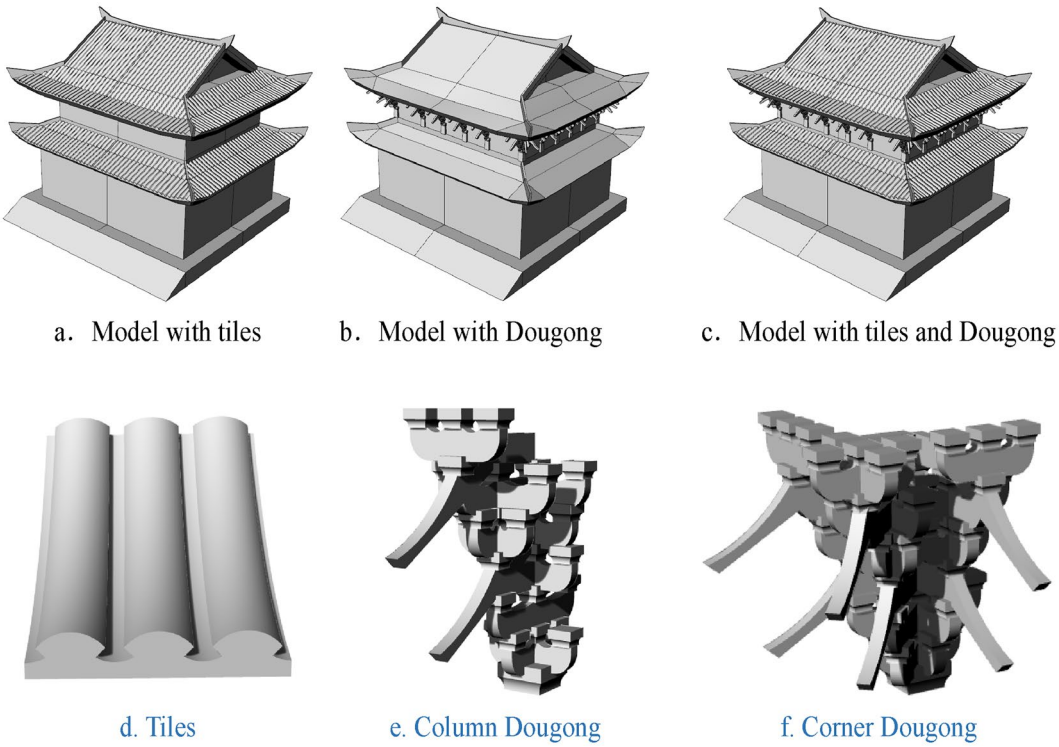

Fig. 10 Geometric models involving different components

floors, and there is a sudden change in wind pressure at the corners, particularly with a significant negative pressure. It means that these parts of the structure are subjected to greater forces and should therefore be emphasized in the design of the preventive protection of the structure. To illustrate the principle, streamtraces around the building are drawn as shown in Fig. 12b, and this phenomenon occurs because the wind stagnates in the middle of the windward side, creating a vortex at the bottom and separation at the top. Besides, on the leeward side, there is significant separation and recirculation of the airflow.

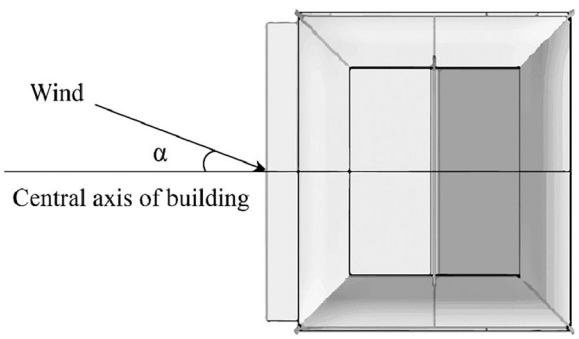

Fig. 11 Wind direction angle

The wind pressure calculation results for different accuracy models were also compared. It can be observed from the wind pressure contours in Fig. 13 that the overall wind pressure distribution patterns are similar for all three accuracy models. For wind directions of 0° and 180°, simplifying the roof shape increases the magnitude of positive pressure on the windward side. However, for other wind directions, this effect is not significant.

Furthermore, the drag coefficients for the different accuracy models were compared. As shown in Fig. 14, the results for 0° are in good agreement with those for 180°. Similarly, the results for 45° closely match those for 135°. This is because the models were mostly symmetrical, with differences only in the stepped portions on the front and back. This indirectly confirms the reliability of the calculation results. The drag coefficients obtained from the three accuracy models are generally similar, with differences not exceeding 3%.

More specifically, the pressure coefficient distribution in specific sections for the different accuracy models were compared. The pressure coefficient is commonly used to characterize wind forces on buildings and is calculated using Eq. (4).

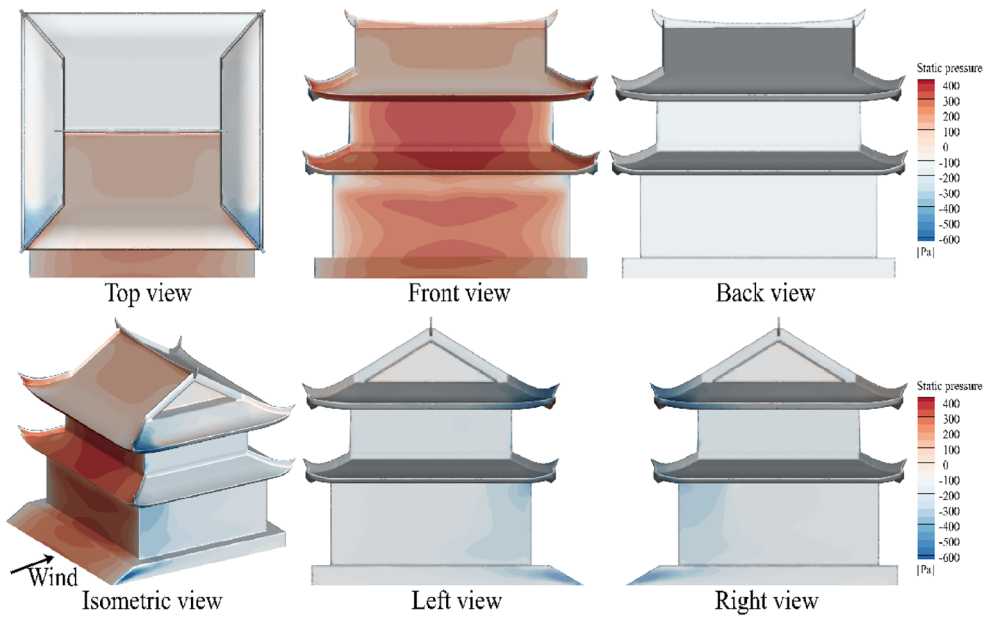

a. Wind pressure distribution

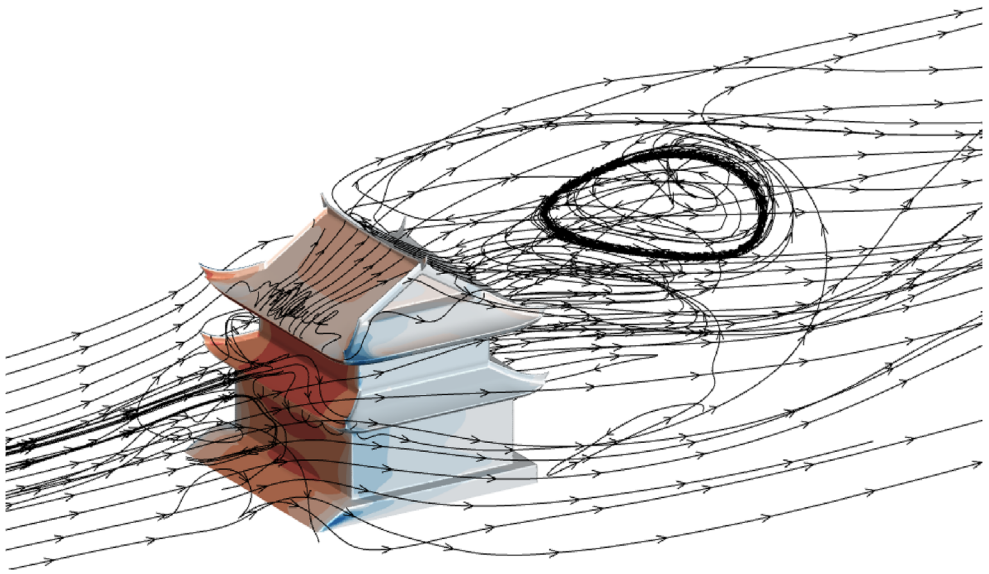

b. Streamtraces around the building

Fig. 12 Wind pressure distribution of the accurate model at 0° wind direction

$$C_{pi} = \frac{P_i}{0.5\rho v^2}. \quad (4)$$

Here, P_i is the pressure at point i without reference wind pressure; ρ is the density of the incoming flow, taken as 1.225 kg/m^3; and v is the wind speed at the reference height. The wind speed of 27.75 m/s at a height of 7.12 m (average height of the roofs) is selected for this study.

As shown in Fig. 15, the pressure coefficient distributions on the cross section for the 50-mm-accuracy model and the accurate model are nearly identical, with a difference of ~ 12.5% at the roof ridge. On the other hand, the 200-mm-accuracy model exhibits a similar

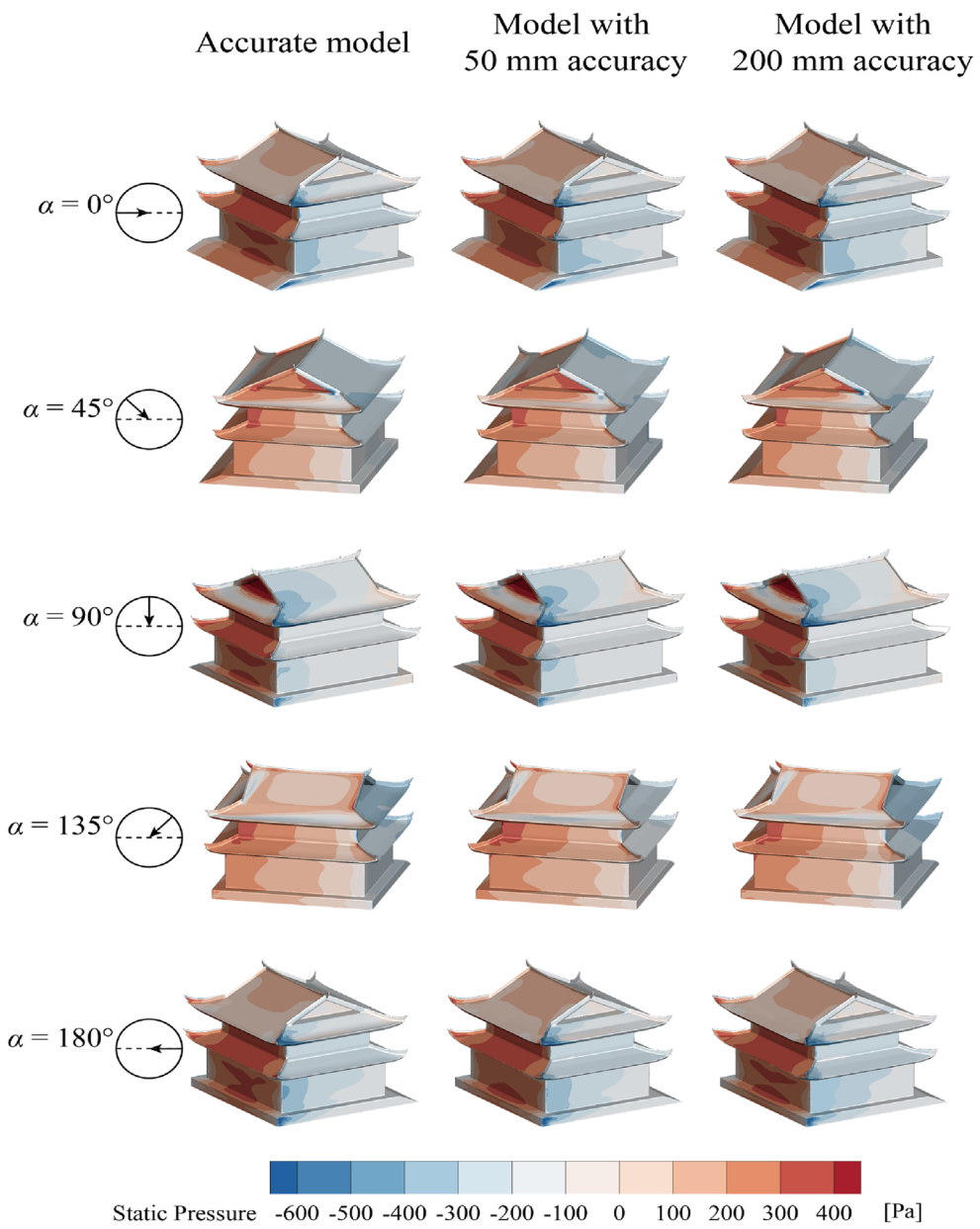

Fig. 13 Wind pressure distribution of different accuracy models

pressure coefficient distribution to the accurate model on sections other than the roof ridge but demonstrates significant divergence at the ridge, with a difference of ~ 47.35%. In particular, at the edges of the roof ridge, the difference reaches as high as 65.18%. The models with the three accuracies demonstrated similar pressure coefficient distributions on the longitudinal section, especially on the leeward side, where there was virtually no difference.

The above results indicate that the simplified method for determining the roof shape is reasonable and effective. However, there should be a certain limit to the simplification of the roof shape. Excessive simplification can lead to a blunt roof shape for traditional timber buildings and may affect the accuracy of CFD calculations. On the other hand, appropriate simplification with adequate accuracy can effectively simplify the roof modeling, saving computational effort while ensuring accuracy. Based on the computational results, it is recommended to adopt

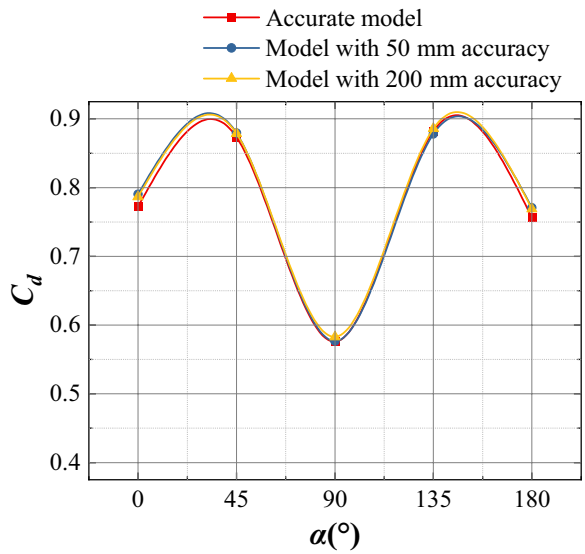

Fig. 14 C_d of different accuracy models

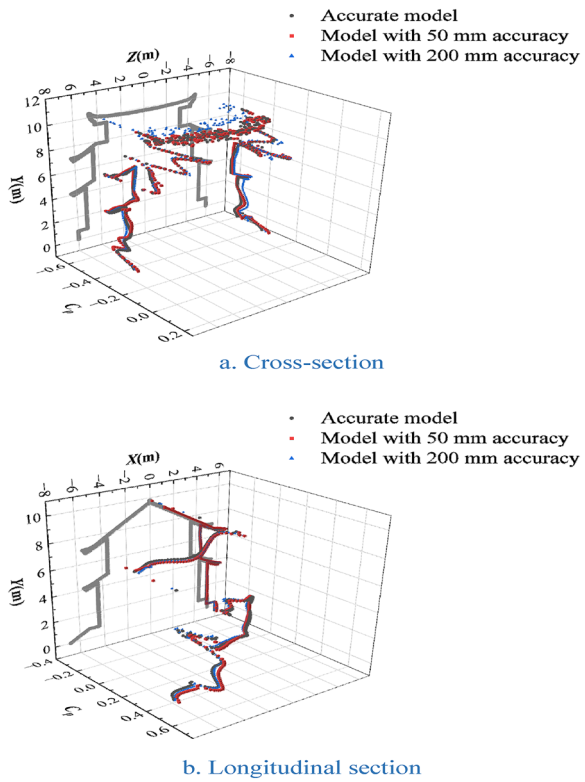

Fig. 15 C_p of different accuracy models at 0° wind direction

a geometric model that replaces the curved roof cornices with a 3-segment polyline in CFD simulation modeling.

The influence of roof tiles and Dougong on wind pressure calculation results

As shown in Fig. 16, the model considering roof tiles exhibits significant differences in wind pressure distribution compared to the original model. On the other hand, the model considering Dougong exhibits a wind pressure distribution that is essentially consistent with the original model. Moreover, the presence of roof tiles reduces the positive pressure on the roof.

Furthermore, comparing the drag coefficients of the models considering different components, as shown in Fig. 17, it is evident that the presence or absence of Dougong has minimal influence on the drag coefficient (within 5%). However, the presence of roof tiles significantly reduces the drag coefficient, with an impact of over 30% at various wind directions. The largest impact is observed at 135°, with a reduction of − 36.35%.

More specifically, analyzing the distribution of wind pressure coefficients on specific sections considering different component models, as shown in Fig. 18, it is clear that the presence of roof tiles significantly affects the wind pressure on the roof, even changing it from negative to positive. At the edges of the eaves, the impact reaches as high as − 265.81%. Therefore, the influence of roof tiles on the wind pressure in the area they cover cannot be ignored.

The above results indicate that it is necessary to consider the influence of roof tiles when analyzing the wind resistance performance of traditional Chinese architecture. The presence of roof tiles alters the distribution of wind pressure, reducing the C_d with a difference of up to 36.35%. On the other hand, the presence or absence of Dougong has a minimal impact on the calculation results. This may be because the Dougong is covered by the eaves and has less influence on the incoming flow.

Analysis of the causes of roof tile impact

The above calculation results indicate that roof tiles have a significant impact on wind pressure calculations for traditional Chinese architecture, especially at the eaves. Given the complexity of building a model containing tiles, to establish a simplified method for tile modeling, this study further explored whether the increase in roof thickness owing to tiles caused the difference in calculation results. A model incorporating the thickness of roof tiles in analysis and computation is shown in Fig. 19.

The pressure contour plots for different wind directions are shown in Fig. 20. It can be observed that adding the thickness of roof tiles to the original model does not effectively simulate the effect of roof tiles. The pressure contour plot of this simplified model with increased

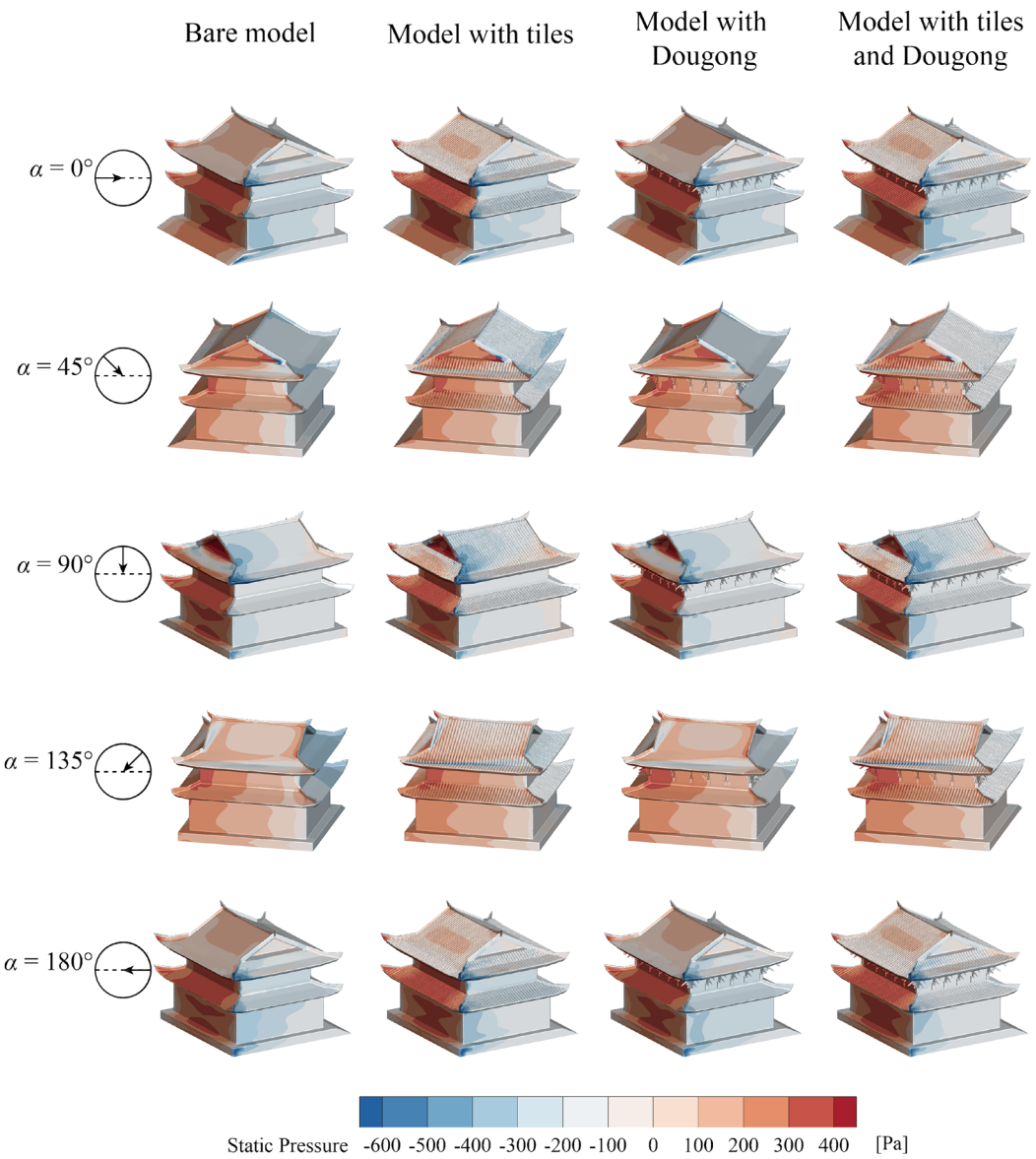

Fig. 16 Pressure distribution of models with different components

roof thickness is closer to that of the original model as opposed to that of the model that includes roof tiles. Furthermore, the analysis of the C_d in Fig. 21 reveals that the simplified model differs from the model with roof tiles by more than 40% for various wind directions, whereas the maximum departure from the original model is only 7.53%. In the analysis of the pressure coefficient distribution on specific sections for the three models in Fig. 22, it is evident that an increase in roof thickness has a minimal impact on the wind pressure distribution, whereas the presence of roof tiles significantly affects the wind pressure distribution on the roof.

Therefore, increasing the roof thickness has a minimal impact on the wind pressure distribution. The presence of roof tiles may primarily affect the building by altering the aerodynamic shape of the building, resulting in an increased Reynolds number and a narrower wake width, leading to a decrease in the C_d.

Conclusions

When conducting wind resistance calculations and studying the wind performance of traditional Chinese timber structures, using CFD simulations to obtain wind pressures on buildings is the most efficient and cost-effective

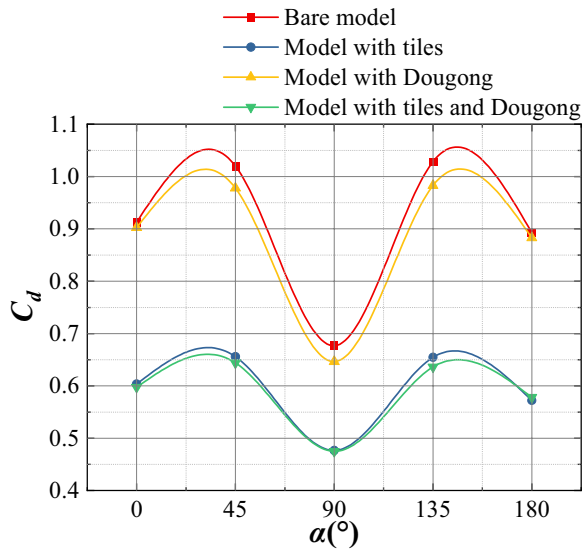

Fig. 17 C_d of models with different components

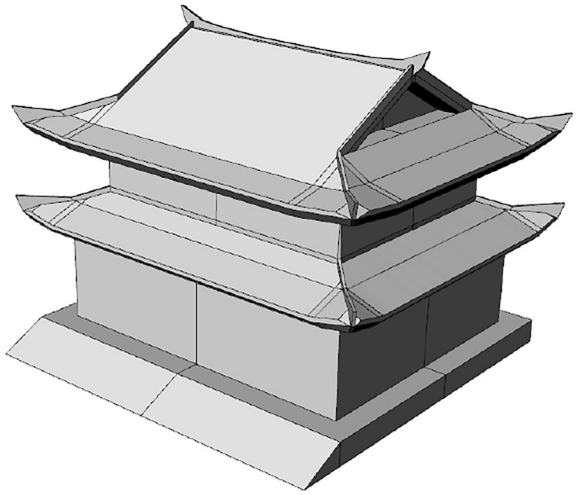

Fig. 19 Model with tile height

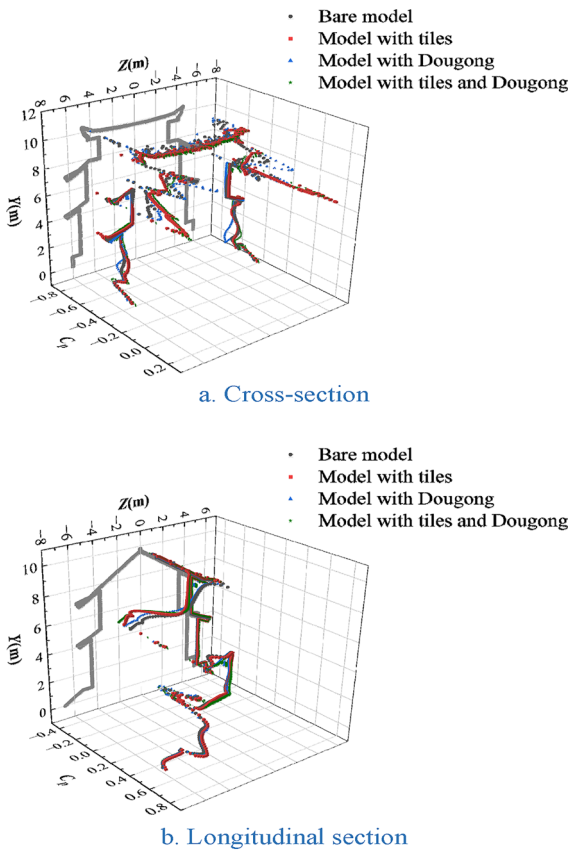

Fig. 18 C_p of models with different components at 0° wind direction

approach. This study focuses on the practical needs of modeling strategies in traditional building wind pressure numerical simulations, selecting the most complex roof form, the double-eave Xieshan roof, and taking the example of Shisi Temple. Using CFD numerical simulations, this study explored the influence of the roof shape, roof tiles, and Dougong on wind pressure calculations for traditional Chinese buildings. This study provides a procedural method for simplifying the roof shape during geometric modeling and offers recommendations for component simplification. The following conclusions are drawn:

(1) Appropriate simplification of the roof shape can improve computational efficiency while meeting the required level of accuracy, which ensures the difference between the drag coefficient of the simplified model and the exact model does not exceed 3%. However, excessive simplification can lead to distorted results, particularly in the ridge section of the roof. Given the large curvature of the roof angles, it is recommended to use a polyline with at least three segments to approximate the original curve.

(2) The influence of roof tiles on the distribution of roof wind pressures cannot be ignored. Their presence can significantly reduce the drag coefficient by more than 30%. The impact of Dougong, located under the eaves, on wind pressure distribution is generally negligible and can be disregarded, and its effect on the drag coefficient does not exceed 5%.

(3) The impact of roof tiles on the building is likely related to altering the aerodynamic shape of the building rather than increasing its thickness.

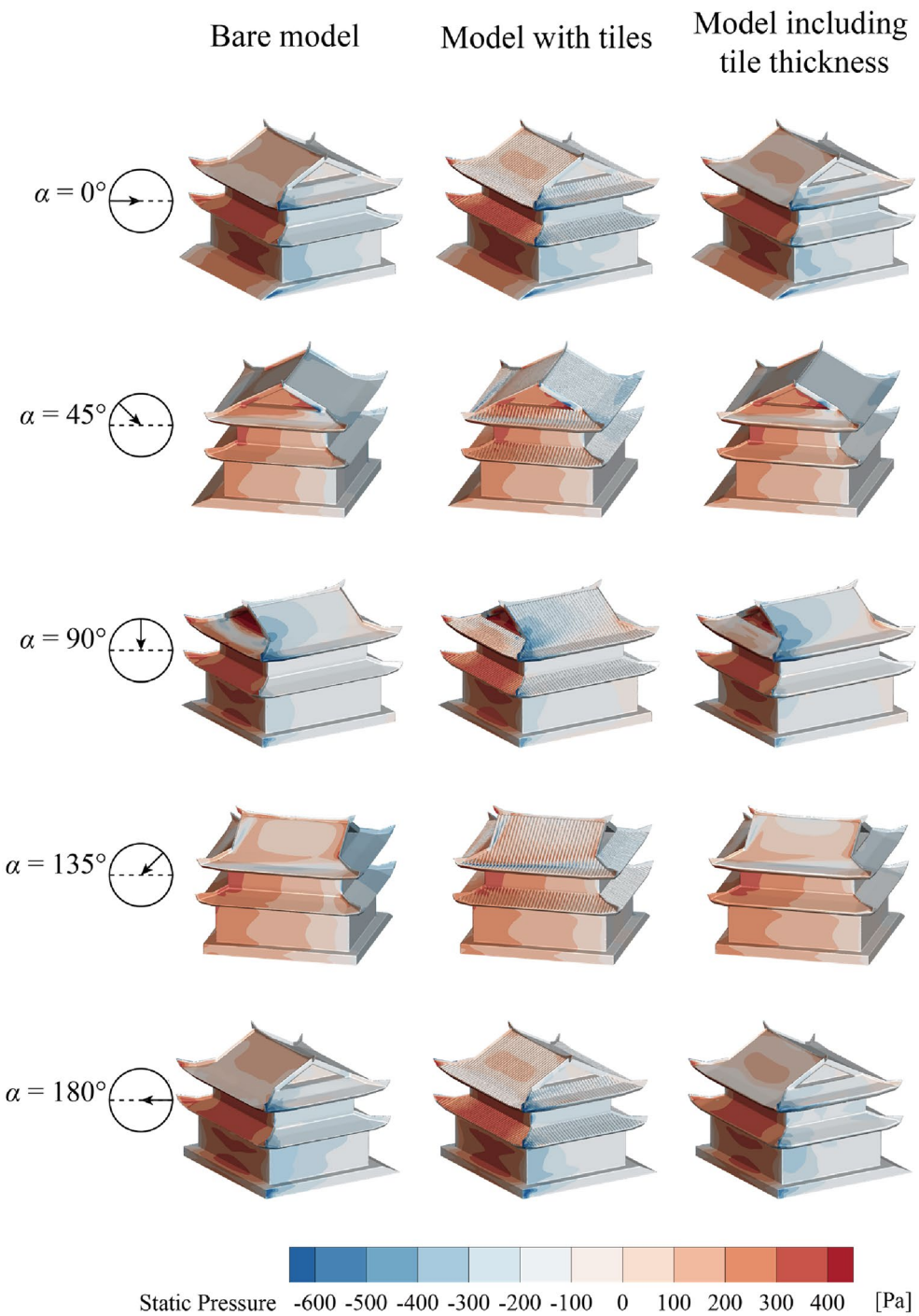

Fig. 20 Wind pressure distribution of models with different tile considerations

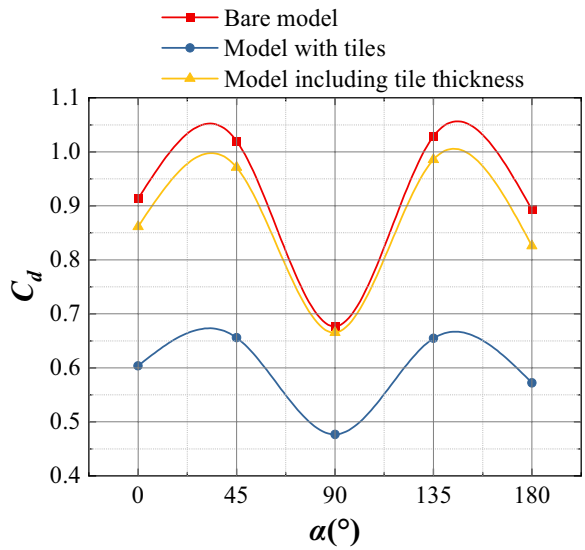

Fig. 21 C_d of models with different tile considerations

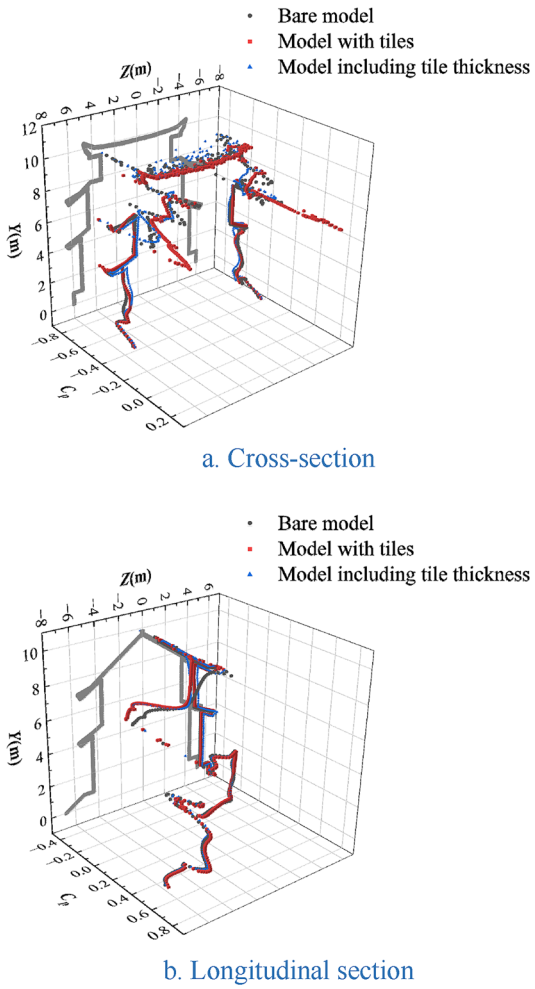

Fig. 22 C_p of models with different tile considerations at 0° wind direction

Therefore, it is important to consider this influence when analyzing the wind resistance of traditional Chinese buildings.

The research findings provide guidance for the geometric modeling of traditional timber structures in wind resistance studies using numerical simulations. This ensures high-accuracy computational results while significantly improving computational efficiency. Owing to time and resource limitations, this study did not explore specific modeling simplification methods for roof tiles. Future work will consider adjusting roof roughness to simulate the effects of roof tiles.

Abbreviations

CFD Computational fluid dynamics
C_d Drag coefficient
C_p Pressure coefficient

Acknowledgements
Not applicable.

Author contributions
XG contributed to the methodology, simulation, results analysis, and original draft of this manuscript. QC and YH contributed to review of this manuscript. All authors read and approved the final manuscript.

Funding
This paper is written with support by Jiangsu Provincial Key Research and Development Program (BE2022833) and Jiangsu Provincial Cultural Relics Research Program (2021SK16).

Availability of data and materials
The datasets used and/or analyzed during the current study are available from the corresponding author on reasonable request.

Declarations

Competing interests
The authors declare that they have no competing interests.

Received: 21 July 2023 Accepted: 25 January 2024
Published online: 10 February 2024

References

1. Erarslan A (2021) An example of traditional timber building techniques from Anatolia. Granary structures in the region of the Eastern Black Sea Turkey; serender. Int Wood Products J 12(1):58–70. https://doi.org/10.1080/20426445.2020.1805688
2. Guchan NS (2007) Observations on earthquake resistance of traditional timber-framed houses in Turkey. Build Environ 42(2):840–851. https://doi.org/10.1016/j.buildenv.2005.09.027
3. Ma S, Chun Q, Zhang C, Yang L, Qian Y, Cao G, Dong Q (2023) Quantitative evaluation method for the structural safety status of traditional courtyard-style timber buildings. Int J Architect Herit. https://doi.org/10.1080/15583058.2023.2221224
4. Murta A, Pinto J, Varum H (2011) Structural vulnerability of two traditional Portuguese timber structural systems. Eng Fail Anal 18(2):776–782. https://doi.org/10.1016/j.engfailanal.2010.12.017
5. Poletti E, Vasconcelos G, Branco JM, Isopescu B (2019) Effects of extreme environmental exposure conditions on the mechanical

behaviour of traditional carpentry joints. Constr Build Mater 213:61–78. https://doi.org/10.1016/j.conbuildmat.2019.04.030
6. Uchida A, Kawai N, Maekawa H (1998) Dynamic characteristics in Japanese traditional timber buildings. In: 5th World Conference on Timber Engineering, Montreux, Switzerland, Aug 17–20; 1998. Pp. 34–41
7. Hwangbo AB (2014) A study on entasis and wooden columnal curvature in the far east—architectural theory of horyuji temple. J Region Assoc Architect Inst Korea 16(3):43–51
8. Delun W, Jinhai W, Yiran F, Zhongzhi W (1991) An experimental research for the wind behavior of a high-rise wooden pagoda in China. J Chongqing Inst Architect Eng 01:15–21
9. Tieying L, Shanyuan Z, Shiwen L (2002) Test analysis for the wind pressure on Yingxian wooden tower. J Exp Mech 03:354–362
10. Tieying L, Shanyuan Z, Shiwen L (2003) Vibration of Yingxian wooden tower under the action of wind. Mech Eng 02:40–42
11. Lin'an W, Weidong H, Xinqun Y (2012) A summary on the research and analysis of testing and monitoring the Yingxian county timber pagoda structure. China Cult Herit Sci Res 03:62–67
12. Li Y, Deng Y, Li A (2022) A nondestructive method for controlling wind loads and wind-induced responses of wooden pagoda. Wind Struct 34(6):525–538. https://doi.org/10.12989/was.2022.34.6.525
13. Li Y, Deng Y, Li A, Xu T (2023) Comparative studies of computational fluid dynamic geometric models at multiple levels of details in evaluating wind action on Asian ancient wooden tower. Int J Architect Herit 17(6):970–987. https://doi.org/10.1080/15583058.2021.2003911
14. Li Y, Sun PP, Li A, Deng Y (2021) Wind effect analysis of a high-rise ancient wooden tower with a particular architectural profile via wind tunnel test. Int J Architect Herit 17(3):518–537. https://doi.org/10.1080/15583058.2021.1938748
15. Yuhang L, Yang D, Aiqun L, Tao X (2021) Investigation on wind pressure and shape factor of high rise ancient Chinese wooden pagoda via wind tunnel test. Eng Mech 38(10):64–73
16. Yuhang L, Yang D, Aiqun L, Tao X (2022) Wind tunnel test and CFD simulation analysis for wind pressure distribution of Yingxian wooden pagoda. J Build Struct 43(03):81–91. https://doi.org/10.14006/j.jzjgxb.2020.0361
17. Hanazato T, Minowa C, Niitsu Y, Nitto K, Kawai N, Maekawa H, Morii M (2010) Seismic and wind performance of five-storied pagoda of timber heritage structure. In: 7th International Conference on Structural Analysis of Historic Constructions, Tongji Univ, Shanghai, PEOPLES R CHINA, Oct 06–08 2010. Advanced Materials Research. pp 79. https://doi.org/10.4028/wwwscientific.net/AMR.133-134.79
18. Hanazato T, Niitsu Y, Morii M, Minowa C, Nitto K, Yokoo T (2016) Seismic and wind performance of five-storied pagoda of timber heritage structure affected by Great East Japan Earthquake of 2011 and typhoon Jelawat of 2012. In: 10th International Conference on Structural Analysis of Historical Constructions (SAHC)—Anamnesis, Diagnosis, Therapy, Controls, Leuven, BELGIUM, Sep 13–15; 2016. pp 1343–1348
19. Xun W, Dai Z, Yu L, Lulu M, Zitong W, Sheng X (2017) Numerical simulationon wind pressure and wind field of Chinese ancient buildings with multiple-eaveand double-pitch roof. J Shanghai Jiaotong Univ (Chin Ed) 51(11):1287–1296. https://doi.org/10.16183/j.cnki.jsjtu.2017.11.002
20. Chengjun B, Zenan C, Ying C, Lingjing H (2021) Research on wind load shape coefficient of Rouyuan building in Jiayuguan. Spec Struct 38(06):61–66. https://doi.org/10.19786/j.tzjg.2021.06.012
21. Han Y, Chun Q, Xu X, Teng Q, Dong Y, Lin Y (2022) Wind effects on Chinese traditional timber buildings in complex terrain: the case of Baoguo Temple. J Build Eng. https://doi.org/10.1016/j.jobe.2022.105088
22. Shan W, Yang Q, Guo K, Tamura Y (2023) Effects of slope curvature, ridge height and layered roofs on wind pressures on traditional-Chinese-style gable-hip and gable roofs. J Build Eng. https://doi.org/10.1016/j.jobe.2023.106300
23. Han Y, Chun Q, Hua Y (2021) Wind-induced vibration of traditional Chinese citygate buildings in the Ming-Qing dynasties—a case study of the Nanjing drum tower. Int J Architect Herit 17(4):615–634. https://doi.org/10.1080/15583058.2021.1953191
24. Han Y, Chun Q, Jin H (2021) Wind-induced vibration performance of early Chinese hall-style timber buildings. J Wood Sci 67 (1). https://doi.org/10.1186/s10086-020-01939-3
25. Li H, Chun Q, Han Y, Jin H, Lin Y, Ashraf M, Corbi O, Yang P, Wang L, Corbi I (2019) Research on wind vibration performance of Chinese early traditional timber structure—a case study of the main hall of Tianning temple. MATEC Web of Conferences 275. https://doi.org/10.1051/matecconf/201927501005
26. Chowdhury AG, Canino I, Mirmiran A, Suksawang N, Baheru T (2013) Wind-loading effects on roof-to-wall connections of timber residential buildings. J Eng Mech 139(3):386–395. https://doi.org/10.1061/(asce)em.1943-7889.0000512
27. Hegyi D, Armuth M, Halmos B, Marotzy K (2022) The effect of wind on historical timber towers analyzed by plastic limit analysis in the focus of a collapse. Eng Failure Anal 134:105852. https://doi.org/10.1016/j.engfailanal.2021.105852
28. Taleb R, Ramanantoa H, Reynolds T, Beckett CTS, Huang Y, Rakotoarivony M, Gagnon AS, Andriamaro L (2023) Fragility assessment of traditional wooden houses in Madagascar subjected to extreme wind loads. Eng Struct 289:116220. https://doi.org/10.1016/j.engstruct.2023.116220
29. TPU Aerodynamic Database (2023) Tokyo Polytechnic University. http://wind.arch.t-kougei.ac.jp/system/eng/contents/code/tpu. Accessed 17 Oct 2023.
30. Standardization CAfEC (2012) Load code for the design of building structures. vol GB 50009-2012. National Standard of the People's Republic of China

Publisher's Note